Chemical Science

ROYAL SOCIETY OF CHEMISTRY

EDGE ARTICLE

View Article Online
View Journal | View Issue

Cite this: *Chem. Sci.*, 2021, **12**, 3644

All publication charges for this article have been paid for by the Royal Society of Chemistry

Received 20th October 2020
Accepted 20th January 2021

DOI: 10.1039/d0sc05780k

rsc.li/chemical-science

Designing caps for colloidal Au nanoparticles†

Xiaoli Tian,[a] Jianpeng Zong,[a] Yusai Zhou,[a] Dapeng Chen,[b] Jia Jia,[a] Shuaibin Li,[a] Xiaochen Dong,[bc] Yuhua Feng*[a] and Hongyu Chen*[a]

The plasmonic property of a nanostructure is highly dependent on its morphology, but there are few methods for appending a domain as the "functional group" or modifier. As a means of modulating plasmonic properties, we create and modulate Au hats on Au nanoparticles, including mortarboards, beret hats, helmets, crowns, antler hats and antenna hats. The structural control arises from the active surface growth as a result of dynamic competition between ligand absorption and metal deposition. It allows the continuous tuning of hat morphologies, from the facet-controlled growth of mortarboards, to the spreading-favored growth of beret hats and helmets, and to the vertical growth of pillars in crowns, antler hats and antenna hats. Among these plasmonic nanostructures, the mortarboards show excellent SERS enhancement of 8.1×10^5, which is among the best in colloidal nanostructures; and the antler hats show the photothermal conversion efficiency of 66.2%, which compares favorably with the literature reports.

Introduction

Plasmonic nanomaterials attract tremendous interest due to their wide applications in energy conversion,[1] sensing,[2] imaging, and photothermal therapy.[3] In comparison to plasmonic metals of Ag, Cu, and Al, Au shows excellent chemical stability, biocompatibility, and rich surface functionality.

The conventional modulation of plasmonics is through the control of size, shape, and aspect ratio of nanomaterials.[4] New approaches include the construction of metal shells on dielectric nanoparticles,[5] the design of narrow gaps *via* nanoshells or nanoplates,[6,7] or the control of island growth on nanoparticles and nanorods.[8–10]

A fundamental control of the appending domain on a seed nanoparticle is *via* their interfacial energy: the wetting growth mode leads to conformal coating on the seed and thus the modulation of plasmonics is essentially the size control. In comparison, the non-wetting growth mode can offer rich structural designs by creating appending domains. It often gives islands on the seed surface, where the number of islands, their shape and extent of wetting, and their location (regioselectivity) are the prime targets of synthetic control.[8]

From the perspectives of synthetic advance, plasmonic modulation needs more synthetic handles and a systematic development is of critical importance. In the literature, reaction kinetics was controlled to grow Ag islands from 1, 3, and 6 faces of Pd cubes;[11] and various degree of Au–Ag Janus nanostructures were synthesized by tuning salt concentration.[12] In our group, we showed that in the growth of Ag on Au seeds, the embedding of strong ligand molecules could be exploited to modulate the Au–Ag interfacial energy,[8b] giving a series of structures from core–shell to eccentric, and then to Janus structures with varying degree of surface coverage. Moreover, ligand and reactant concentrations were modulated to influence the "depletion sphere", and thus control the number of Au islands on Au nanoparticles (NPs)[8a] and nanorods.[10]

In this work, we systematically study the growth of Au caps on Au seeds by simultaneous use of a hydrophobic thiol ligand and a surfactant. This combination achieves powerful control of the active surface, leading to a dynamic modulation of the spreading and vertical growth of the Au caps. As such, the method offers a wide variety of caps from mortarboards, beret hats, helmets, crowns, antler and antenna hats.

Results and discussion

The prerequisite for tuning cap morphology is the stable and monodispersed AuNPs. For high uniformity, we chose the citrate-stabilized AuNPs of 60 nm diameter (Fig. S4†) as the model system.[13] A strong hydrophobic ligand 4,5-diphenyl-2-imidazolethiol (DPI, Fig. S3a†) was used in combination with a cationic surfactant myristyltrimethylammonium bromide

[a]*Institute of Advanced Synthesis, School of Chemistry and Molecular Engineering, Jiangsu National Synergetic Innovation Centre for Advanced Materials, Nanjing Tech University, Nanjing 211816, China. E-mail: iashychen@njtech.edu.cn; ias_yhfeng@njtech.edu.cn*

[b]*Key Laboratory of Flexible Electronics (KLOFE) and Institute of Advanced Materials (IAM), Institution School of Physical and Mathematical Sciences, Nanjing Tech University, Nanjing 211800, China*

[c]*School of Chemistry and Materials Science, Nanjing University of Information Science & Technology, Nanjing 210044, China*

† Electronic supplementary information (ESI) available. See DOI: 10.1039/d0sc05780k

(MTAB). As direct ligand exchange between citrate and DPI causes serious aggregation, we first replace the citrate with MTAB. The resulting mixture is highly stable and used as the stock solution for all of the subsequent syntheses. Then, DPI was added to functionalize the Au surface. There was no aggregation as indicated by the absence of color change and no longitudinal peak at long wavelength (600–800 nm) (Fig. S5†), and it is further confirmed by electron microscopy (Fig. S6†). Using the functionalized AuNPs as seeds, $HAuCl_4$ was reduced by 2,7-dihydroxynaphthalene (DHN, Fig. S3b†) at different pH. The products were isolated by centrifugation and characterized by transmission electron microscopy (TEM) and scanning electron microscopy (SEM).

When the concentration of NaOH ([NaOH]) is 0.825 mM, a domain was grown from the side of each Au seed (Fig. 1b and S7†). 64% of the domains were nanoplate, and the rest were polyhedrons (Fig. S8†). 68% of nanoplate attached tangent to the spherical seeds *via* its center. It is named mortarboard for the structural similarity. In SEM images, some of the mortarboard nanoparticles were found standing sideway (Fig. 1d), revealing that the nanoplate is about 27 nm in thickness. In the literature, it is known that plates are generally formed as a result of twin plane.[14] The favorable growth at the concave edges leads to anisotropic growth to give triangular plate. When there are two stacking twin planes, all six edges are equally favored, leading to hexagonal plates. In overall consideration, the strong thiolated ligand renders a high surface energy on the seeds, making uniform over-coating growth unfavorable.[15] Basically, it is still an island-growth mode initiating from a single point of the seed,[8] except that the emerging domain is a plate rather than the typical near-spherical island. From the HRTEM image (Fig. 1h and i), the measured 0.234 nm lattice spacing is consistent with the reported distance between Au (111) planes, indicating that the planar surface of the nanoplate is Au (111) facet.[16] The appearance of the weak forbidden 1/3(422) diffraction in SAED (triangle framed spot in Fig. 1j) can be assigned to the presence of planar twin plane parallel to the Au (111) surface.[17]

DHN is used as the reductant in our method. As shown from the chemical equations (eqn (1) and (2)), the oxidation of DHN gives lots of protons. The NaOH promotes the reaction by neutralization. With increase of [NaOH], the reaction accelerates as indicated by the rate of color change. Thus, we use [NaOH] as a variable for tuning the structural features.

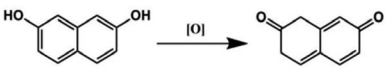

(1)

$$3C_{10}H_8O_2 + 2HAuCl_4 = 3C_{10}H_6O_2 + 2Au + 8Cl^- + 8H^+ \quad (2)$$

When [NaOH] was increased to 3.96 mM, the initial color change occurred at 2 min, much faster than the 10 min of the above reaction. Instead of nanoplate, the emerging Au domain became thicker with an obvious curvature, appearing as a helmet on the seed nanoparticle (Fig. 1c and S9†). Its inner surface nearly matches the curvature of the seed, with larger gap at its perimeter. The helmet cover about 1/4 to 1/2 of the seed surface and the gap size is non-uniform. Occasionally a bridge is discernable between the concave surface of the cap and the convex surface of the seed, indicating that the helmets are grown from the seeds rather than from guest–host recognition (Fig. 1f).

The helmet and the mortarboard are distinctively different growth modes. To explore the intermediate states between them, we carried out a series of reaction with intermediate [NaOH]. The percentage of plates decreases with the increase of [NaOH] (Fig. S10†) and at [NaOH] = 2.64 mM, most of the caps are short beret hats with no plate (Fig. 1e, S11 and S8†). In comparison to helmets, the thickness of the beret hats and helmets are similar, with the main differences being the coverage of the seed.

The growth of island domain on a seed is essentially a solid–solid wetting phenomenon. In the literature, when a metal domain is directly grown on a metal seed, it is often the wetting growth mode.[18] When a metal domain is grown on the ligand-covered metal surface, it is often the non-wetting growth mode.[8,12,19] A wetting growth mode on the ligand layer is quite rare.[6,20] In this work, the clear gap is indicative of the ligand layer. It is likely that DPI binds strongly to the Au surface and then MTAB adsorption renders the seed surface favourable for the emerging Au domain (Fig. 1a).

Obviously, the helmet cannot form instantaneously, but gradually grow in size and coverage. The flattened domain with

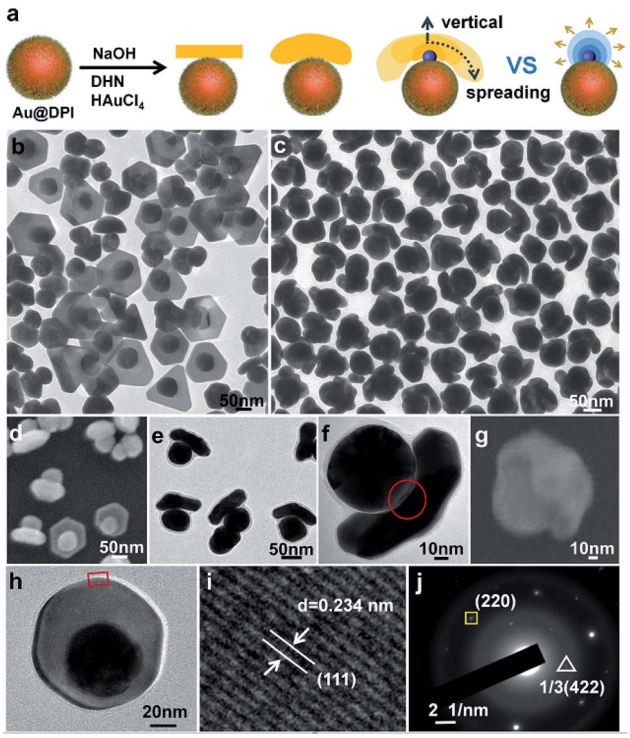

Fig. 1 (a) Schematics illustrating the synthesis of mortarboard, helmet and beret hat. TEM and SEM images of mortarboard, helmet and beret hat prepared under different concentration of NaOH: (b and d) 0.83 mM, (c, f and g) 3.96 mM and (e) 2.64 mM. (h and i) TEM, HRTEM and (j) SAED of a single mortarboard nanoparticle.

matching curvature is defined as the spreading growth mode. On the other hand, increasing the thickness of the helmet is defined as the vertical growth (Fig. 1a). In the macroscopic world, for a droplet of liquid on a flat substrate, its contact angle determines its overall shape as the liquid could quickly reshape to minimize its surface energy. In contrast, the solid island domain here cannot reshape and is highly dependent on the growth kinetics. As such, its inner curvature meeting the seed is determined by the degree of wetting, whereas its outer surface or overall shape is determined by the growth kinetics. In the typical island growth mode, the emerging domain grows outward from the seed, giving a spheroidal island (chef's hat, Fig. 1a).[8] In forming the helmet, however, it appears that the spreading growth is greatly more favourable than the vertical growth, likely due to active growth sites at its perimeter (Fig. 1a).

In our previous study, we used the dynamic adsorption of a strong thiol ligand to modulate the growth of Ag on Au seeds. It is easier for Ag to deposit on an emerging domain with few ligands, than an existing domain with well packed ligands.[8b] With the growth competition, the fresh surface would become fresher after the growth, whereas the old surface becomes older. Exploiting such an active surface growth mode gives the (Au sphere)–(Ag wire)–(Ag plate) triblock nanostructure.[21]

The presence of active surface can explain the preferred spreading growth and hence, the beret hats and helmets appear flattened in comparison to the chef's hat. We hypothesize that a growth site near the seed would experience steric hindrance for the ligand adsorption (DPI and MTAB), making the deposition of Au atoms more favorable. As the growth competition makes the perimeter fresher, the outer surface becomes older with ligand inhibition (Fig. 2a). In other words, the spreading growth is the result of two factors: a wetting growth mode and an active surface at the perimeter. The rapid growth at the active surface is also expected to cause the hat perimeter to occasionally deviate from the seed curvature, leading to non-uniform gaps.

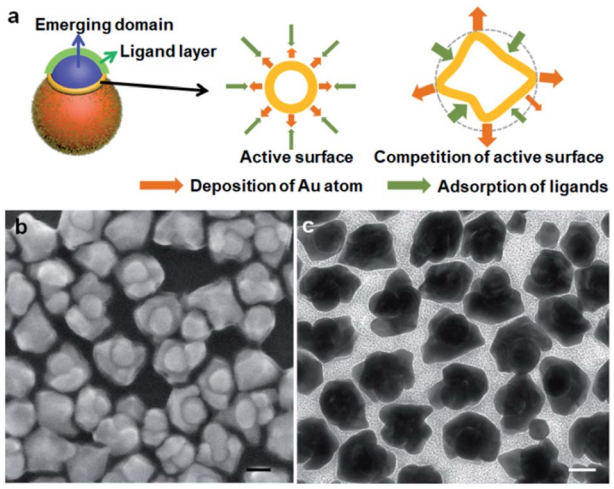

Fig. 2 (a) Schematics illustrating the active surface growth; (b and c) TEM and SEM images of the helmet synthesized by using 5 times diluted seed solution. Scale bars: 50 nm.

The dynamic competition between the Au deposition and ligand inhibition is the critical factor. The outcome with varying reduction rates leads to the different morphologies of the new Au domains. At the lower reduction rate, the ligand inhibition wins the competition, selectively blocking the Au (111) surface and leading to the formation of mortarboards: if a twin plane[14] develops randomly in the newly formed Au domain, we would expect a random nanoplate orientation which is against the high ratio of the tangent mortarboards (44%). It is likely that the extension of the (111) facet from the seed, upon inhibition by the strong DPI, develops a twin plane parallel to the (111) facet, so that the resulting nanoplate becomes tangent. The 20% of the nanoplates attached to the side of the seeds may arise from the independently developed new Au domain with random twinning. As the twining did not occur in all the nuclei, the remaining 36% of the Janus nanostructures did not show plate morphology.

When the beret hat grows larger into helmets, it is conceivable that there is also competition between the active growth sites along the perimeter. The side-view of the helmet in SEM images (Fig. 1g) shows non-uniform expansion of its perimeter, giving helmets with petals, which are indicative of differentiating active surface. As some sites become fresher and some older, the differentiation would explain the non-uniform spreading and the formation of petals (Fig. 2a).

To push for the limit of spreading growth, we tried to increase the amount of Au growth on each seed. The reactants were kept at the same concentration to maintain the growth mode, whereas the amount of seeds was reduced to 1/5 of the standard condition. The helmet coverage increased to about 3/4 of the seed surface (Fig. 2b and c), agreeing with the active surface mode. But the overly grown petals showed facets that disrupt the overall helmet shape.

Further increase of [NaOH] to 6.6 mM did not lead to obvious structural changes (Fig. S12†). Thus, to increase the rate of reduction, we attempted to increase the concentration of the reductant DHN. While the emerging hat is still on the seed, its shape evolves to completely different forms as follows. At [NaOH] = 3.96 mM and [DHN] = 4.61 mM, the hats showed multiple vertical pillars attached to a curving hat that matches with the seed surface (Fig. 3b and S13†). In other words, there is sign of vertical active surface growth in addition to the spreading growth. While all seeds grew pillars, their number is non-uniform in the sample: 73% of the nanoparticles have well-developed crowns with 5–12 pillars of average length of 42 nm, and 18% of them contain a small crown with 1–3 pillars (Fig. S8†).

When the [DHN] reached 9.23 mM, it appears that the vertical growth dominated the initial stage, form a stem (24 nm) before spreading horizontally (Fig. 3c). Such antler hats have 5–12 pillars with an average length of 54 nm. The inner edge facing the seed does not match the curvature of the seed. Apparently it is caused by the crowding of the pillars rather than a wetting phenomenon. From the SEM images (Fig. 3e and S14†), 32% of the antler hats are coplanar, whereas the pillars of the remaining hats extend more randomly (Fig. S8†). We believe that the lattice structure of the initial stem is critical: should

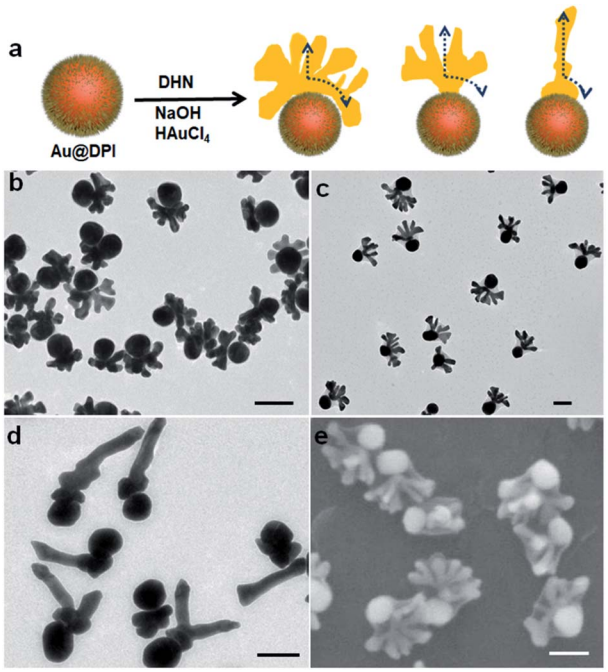

Fig. 3 (a) Schematics illustrating the growth of crown, antler hats and antennas. TEM images of the (b–d) crown, antler hats and antennas prepared under different concentration of DHN reductant: (b) 4.61, (c) 9.23 and (d) 13.8 mM. (e) SEM image of antler hats in c. Scale bars: 100 nm.

a twinning defect be developed in the stem, the subsequent growth would be restricted by the plate morphology, even with the vertical and spreading active sites. At [DHN] = 13.8 mM, 77% of the hats became more like antennae, with a main pillar (average length 120 nm) and multiple smaller twigs on its surface (Fig. 3d, S15 and S8†). Hence, the vertical growth dominates the growth process, and the spreading growth only contributed to the formation of twigs.

There are clear trends in the evolution from crown to antler and antenna hats: with faster Au reduction, the vertical growth becomes increasingly more preferred over the spreading growth (Fig. 3a). As the helmet grows to a certain size, the active sites on its perimeter would be too far from its center. Hence, above the helmet and near its center, the chemical reaction producing the growth material (Au atoms) would be faster than its depletion by diffusion. This build up in concentration eventually gives an active site which leads to a vertical pillar. As the vertical growth continues, more pillars would emerge from regions of high over-saturation. Overall, there are two levels of dynamic competition: the competition between the vertical and spreading growth; and the competition among the pillars and among the growth sites (petals) along the perimeter. The first level of competition is well supported by the clear trend among the samples switching from spreading to vertical growth. The splitting of the active sites is highly unusual for colloidal growth of nanoparticles,[22] yet it fits well with the second level of competition in our hypothesis.

To investigate the structural details, HRTEM measurement of crown were carried out. The ordered lattice fringe at Au-crown interface, and the same orientation of FFT patterns of squared areas, indicate the probable epitaxial growth of crown on seed (Fig. 4a–g). It appears that the periphery of the active surface is inhibited by ligand and affected by dynamic competition, but the internal lattice remains at the same direction. Such a growth mode was reported in our previous work and is typical of the active surface growth.[21]

The measured lattice spacing is consistent with the reported distance among the Au (111) planes (Fig. 4h–j).[16] Energy-dispersive X-ray spectroscopy (EDS) elemental mapping confirmed the uniform distribution of Au, S, and N elements (Fig. 4k–o), thus the presence of DPI thiol ligand and MTAB surfactant on the surface of crown structure can be verified.[23]

The control of hat morphology is a new means to modulate the plasmonic properties of the metal nanostructures. The first series of tuning [NaOH] led to mostly "normal" hat morphologies, from the rigid mortarboard to the conformal beret hat and helmet, all of which have no outward protrusion. In the UV-Vis spectra, all three structures showed broad absorption from 600–800 nm, consistent with their anisotropic features (Fig. 5a). The mortarboard has the highest longitudinal absorption, which can be attributed to the in-plane dipole.[17] The beret hat and helmet are expected to have improved SERS performance considering their large area of narrow gaps. While their SERS signals are indeed stronger (about 10 times) than the Au seeds, they are not exceptional, likely because the combination of DPI and MTAB gave too large a gap (2–5 nm). In comparison, the mortarboard has the strongest SERS (about 200 times stronger than the DPI-coated seeds of equal concentration). It may arise from the resonance with the 785 nm laser used in the SERS measurement (Fig. 5b). The enhancement factor (EF) is estimated to be 8.1×10^5. While this value is moderate for dried samples on a substrate, it is among the largest for colloidal Au

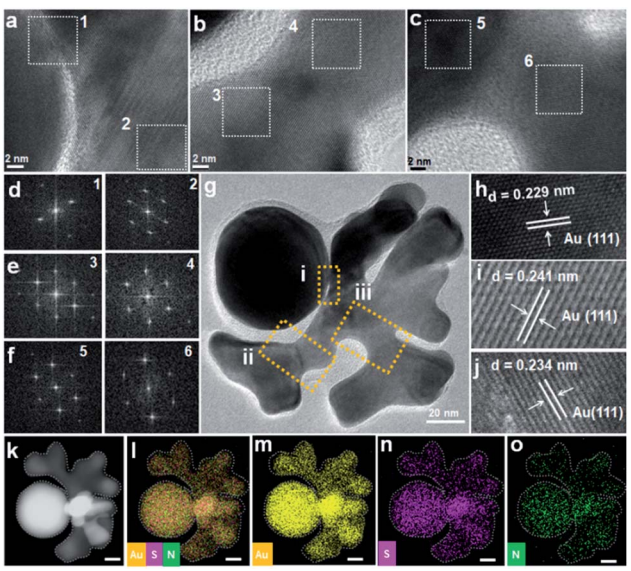

Fig. 4 (a–c) HRTEM images, (d–f) FFT of an individual Au crown particle (g). (h–j) Measured lattice spaces of the squared areas (i–iii in (g)). (k–o) Elemental mapping of an Au crown particle. Scale bars: 10 nm.

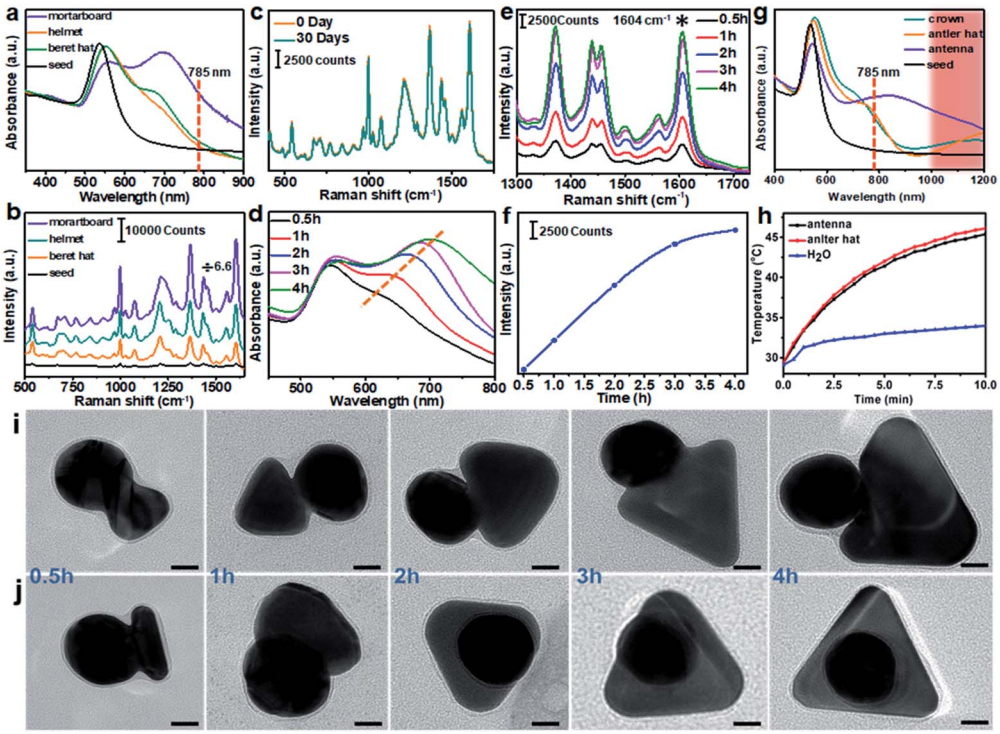

Fig. 5 (a) Absorption spectra of mortarboard, helmet and beret hat. (b) SERS of mortarboard, helmet, beret hat and Au seed with the same concentration. The SERS intensity of the helmet was scaled down by 6.6 times. (c) Demonstration of the SERS stability of mortarboard solution after 30 days. (d) Absorption spectra of mortarboard grew for different times. (e and f) SERS of 1604 cm^{-1} peak for mortarboard structure at different growth time. (g) Absorption spectra of crown, antler hat and antennas. (h) Photothermal heating curves of antler hats, antennas, and water under 1 W cm^{-2} laser irradiation. (i and j) TEM images of mortarboard at different growth time. Scale bars: 20 nm.

samples, where the previous record was nanoplates with EF of 1 $\times$ 10^5, Au–Ag heterodimer (snowman) with 1.6 $\pm$ 0.4 $\times$ 10^6, the dimers and trimers of 15 nm Ag nanoparticles with 10^5 and islands-on-plate with 2.3 $\times$ 10^5.[12,24,25]

With increase of reaction time (0.5–4 h), SERS of the resulting mortarboards increased (Fig. 5e and f). As the plate size also increased (Fig. 5i and j), it is likely the SERS enhancement was a result of increasing absorption. As previously reported, the absorption peak of plates red shifts with increasing plate size.[17] Its improving resonance with the 785 nm laser thus leads to higher intensities (Fig. 5d). Considering that the mortarboard sample showed weaker 785 nm absorption than the neat Au plates (Fig. S16† and ref. 24*a*), the hotspot between the seed and the plate probably also contributes significantly to its SERS intensity. In the literature, most of the SERS studies are carried out for dried samples on a substrate surface,[26] where the SERS intensity is highly site-dependent. In comparison, measurement of colloidal samples would give highly consistent intensity data,[25] because the number of nanostructures in the focal volume is often large enough to average out their individual differences. In comparison to the confocal Raman spectrometer with ultra-small focal volume and intense laser, the portable Raman spectrometer used in this study has a larger focal volume and thus more steady intensity data, as demonstrated in Fig. 5c. According to the recommended standards in a recent review,[27] our Janus structures can fit into "reproducible and reliable" SERS substrates.

While the absence of aggregation would be disadvantageous for SERS intensity, the reliable SERS signals are more representative for comparing the series of nanostructures, as opposed to their random aggregates from the drying process. The second series of tuning [DHN] led to most "decorated" hat morphologies, from crown to antler and antenna hats, all with obvious outward protrusions. The most prominent feature in the UV-Vis spectra is the absorption at long wavelength of 800–1200 nm (Fig. 5g). Despite the higher absorbance at 785 nm, their SERS intensities are all weaker than the above normal hats, likely due to the absence of hotspot (Fig. S17†). But their stronger absorbance makes them advantageous for NIR-II window photo-thermal therapy applications.

Under 1060 nm laser (1 W cm^{-2}), the antler hat showed the best performance, increasing the solution temperature by over 15 °C in 10 min (Fig. 5h). The photo-thermal conversion efficiencies (PCEs) of antler and antenna hats were estimated to be 66.2% and 53.3%, respectively.[28] The former compares favorably with the literature values, and is very close to the 67% efficiency of our recent work (Table S2†).[10]

Conclusions

In summary, we show that the active surface growth is an effective method to create structural variety in the appending domain of Au seeds. In contrast to the wetting growth that leads

to encapsulating shells and the non-wetting growth that leads to appending spheres, the active surface growth creates dynamic competitions between the growth sites. From the facet-controlled growth of mortarboards, to the spreading growth of beret hats and helmets, to the vertical growth of pillars in crowns, antler hats, and antenna hats, the competition between the spreading and vertical growth, and the competition among the neighboring growth sites are the underlying reasons for the rich growth modes.

Conflicts of interest

There are no conflicts to declare.

Acknowledgements

This work was financially supported by the National Natural Science Foundation of China (21673117 and 91956109), Jiangsu Provincial Foundation for Specially-Appointed Professor, start-up fund at Nanjing Tech University (39837102 and 39837140) and SICAM Fellowship from Jiangsu National Synergetic Innovation Center for Advanced Materials.

Notes and references

1 J. Gargiulo, R. Berté, Y. Li, S. A. Maier and E. Cortés, *Acc. Chem. Res.*, 2019, **52**, 2525–2535.
2 H. Malekzad, P. S. Zangabad, H. Mohammadi, M. Sadroddini, Z. Jafari, N. Mahlooji, S. Abbaspour, S. Gholami, M. G. Houshangi and R. Pashazadeh, *TrAC, Trends Anal. Chem.*, 2018, **100**, 116–135.
3 Y. Hernández and B. C. Galarreta, in *Nanomaterials for Magnetic and Optical Hyperthermia Applications*, Elsevier., 2019, pp. 83–109.
4 (*a*) H. Chen, L. Shao, Q. Li and J. Wang, *Chem. Soc. Rev.*, 2013, **42**, 2679–2724; (*b*) M. Grzelczak, J. Pérez-Juste, P. Mulvaney and L. M. Liz-Marzán, *Chem. Soc. Rev.*, 2008, **37**, 1783–1791.
5 (*a*) J. Song, B. Duan, C. Wang, J. Zhou, L. Pu, Z. Fang, P. Wang, T. T. Lim and H. Duan, *J. Am. Chem. Soc.*, 2014, **136**, 6838–6841; (*b*) S. J. Oldenburg, R. D. Averitt, S. L. Westcott and N. J. Halas, *Chem. Phys. Lett.*, 1998, **288**, 243–247.
6 (*a*) D.-K. Lim, K.-S. Jeon, J.-H. Hwang, H. Kim, S. Kwon, Y. D. Suh and J.-M. Nam, *Nat. Nanotechnol.*, 2011, **6**, 452–460; (*b*) Y. Zhang, Y. Gu, J. He, B. D. Thackray and J. Ye, *Nat. Commun.*, 2019, **10**, 1–12.
7 (*a*) T. Jiang, G. Chen, X. Tian, S. Tang, J. Zhou, Y. Feng and H. Chen, *J. Am. Chem. Soc.*, 2018, **140**, 15560–15563; (*b*) Y. Gao, Y. Li, Y. Wang, Y. Chen, J. Gu, W. Zhao, J. Ding and J. Shi, *Small*, 2015, **11**, 77–83; (*c*) J. Chen, Y. Bai, J. Feng, F. Yang, P. Xu, Z. Wang, Q. Zhang and Y. Yin, *Angew. Chem., Int. Ed.*, 2020, DOI: 10.1002/anie.202011334.
8 (*a*) Y. Feng, Y. Wang, X. Song, S. Xing and H. Chen, *Chem. Sci.*, 2017, **8**, 430–436; (*b*) Y. Feng, J. He, H. Wang, Y. Y. Tay, H. Sun, L. Zhu and H. Chen, *J. Am. Chem. Soc.*, 2012, **134**, 2004–2007.
9 J. Huang, C. Liu, Y. Zhu, S. Masala, E. Alarousu, Y. Han and A. Fratalocchi, *Nat. Nanotechnol.*, 2016, **11**, 60–66.
10 J. Jia, G. Liu, W. Xu, X. Tian, S. Li, F. Han, Y. Feng, X. Dong and H. Chen, *Angew. Chem., Int. Ed.*, 2020, **59**, 14443–14448.
11 C. Zhu, J. Zeng, J. Tao, M. C. Johnson, I. Schmidt-Krey, L. Blubaugh, Y. Zhu, Z. Gu and Y. Xia, *J. Am. Chem. Soc.*, 2012, **134**, 15822–15831.
12 J.-H. Lee, M.-H. You, G.-H. Kim and J.-M. Nam, *Nano Lett.*, 2014, **14**, 6217–6225.
13 Y. Feng, Y. Wang, H. Wang, T. Chen, Y. Y. Tay, L. Yao, Q. Yan, S. Li and H. Chen, *Small*, 2012, **8**, 246–251.
14 J. E. Millstone, S. J. Hurst, G. S. Métraux, J. I. Cutler and C. A. Mirkin, *Small*, 2009, **5**, 646–664.
15 Y. Wang, J. He, C. Liu, W. H. Chong and H. Chen, *Angew. Chem., Int. Ed.*, 2015, **54**, 2022–2051.
16 S. Ye, A. P. Brown, A. C. Stammers, N. H. Thomson, J. Wen, L. Roach, R. J. Bushby, P. L. Coletta, K. Critchley, S. D. Connell, A. F. Markham, R. Brydson and S. D. Evans, *Adv. Sci.*, 2019, **6**, 1900911.
17 L. Chen, F. Ji, Y. Xu, L. He, Y. Mi, F. Bao, B. Sun, X. Zhang and Q. Zhang, *Nano Lett.*, 2014, **14**, 7201–7206.
18 Y. Xia, X. Xia and H.-C. Peng, *J. Am. Chem. Soc.*, 2015, **137**, 7947–7966.
19 J. Huang, Y. Zhu, C. Liu, Z. Shi, A. Fratalocchi and Y. Han, *Nano Lett.*, 2016, **16**, 617–623.
20 L. Lin, Q. Zhang, X. Li, M. Qiu, X. Jiang, W. Jin, H. Gu, D. Y. Lei and J. Ye, *ACS Nano*, 2018, **12**, 6492–6503.
21 Y. Feng, Y. Wang, J. He, X. Song and H. Chen, *J. Am. Chem. Soc.*, 2015, **137**, 7624–7627.
22 Y. Wang, J. He, S. Yu and H. Chen, *Small*, 2016, **12**, 930–938.
23 W. Shen, X. Lin, C. Jiang, C. Li, H. Lin, J. Huang, S. Wang, G. Liu, X. Yan, Q. Zhong and B. Ren, *Angew. Chem., Int. Ed.*, 2015, **54**, 7308–7312.
24 (*a*) L. Scarabelli, M. Coronado-Puchau, J. Giner-Casares, J. Langer and L. Liz-Marzán, *ACS Nano*, 2014, **8**, 5833–5842; (*b*) G. Wang, Y. Liu, C. Gao, L. Guo, M. Chi, K. Ijiro, M. Maeda and Y. Yin, *Chem*, 2017, **3**, 678–690.
25 G. Chen, Y. Wang, M. Yang, J. Xu, S. J. Goh, M. Pan and H. Chen, *J. Am. Chem. Soc.*, 2010, **132**, 3644–3645.
26 J. Langer, D. Jimenez de Aberasturi, J. Aizpurua, R. A. Alvarez-Puebla, B. Auguié, J. J. Baumberg, G. C. Bazan, S. E. J. Bell, A. Boisen, A. G. Brolo, J. Choo, D. Cialla-May, V. Deckert, L. Fabris, K. Faulds, F. J. García de Abajo, R. Goodacre, D. Graham, A. J. Haes, C. L. Haynes, C. Huck, T. Itoh, M. Käll, J. Kneipp, N. A. Kotov, H. Kuang, E. C. Le Ru, H. K. Lee, J.-F. Li, X. Y. Ling, S. A. Maier, T. Mayerhöfer, M. Moskovits, K. Murakoshi, J.-M. Nam, S. Nie, Y. Ozaki, I. Pastoriza-Santos, J. Perez-Juste, J. Popp, A. Pucci, S. Reich, B. Ren, G. C. Schatz, T. Shegai, S. Schlücker, L.-L. Tay, K. G. Thomas, Z.-Q. Tian, R. P. Van Duyne, T. Vo-Dinh, Y. Wang, K. A. Willets, C. Xu, H. Xu, Y. Xu, Y. S. Yamamoto, B. Zhao and L. M. Liz-Marzán, *ACS Nano*, 2020, **14**, 28–117.
27 S. E. J. Bell, G. Charron, E. Cortés, J. Kneipp, M. L. de la Chapelle, J. Langer, M. Procházka, V. Tran and S. Schlücker, *Angew. Chem., Int. Ed.*, 2020, **59**, 5454–5462.

28 (*a*) D. Chen, Z. Zhong, Q. Ma, J. Shao, W. Huang and X. Dong, *ACS Appl. Mater. & Inter.*, 2020, **12**, 26914–26925; (*b*) P. Liang, H. Tang, R. Gu, L. Xue, D. Chen, W. Wang, Z. Yang, W. Si and X. Dong, *Sci. China. Mater.*, 2019, **62**, 1199–1209; (*c*) D. Chen, Y. Tang, J. Zhu, J. Zhang, X. Song, W. Wang, J. Shao, W. Huang, P. Chen and X. Dong, *Biomaterials*, 2019, **221**, 119422; (*d*) Z. Yin, D. Chen, J. Zou, J. Shao, H. Tang, H. Xu, W. Si and X. Dong, *ChemistrySelect*, 2018, **3**, 4366–4373.